CHAPTER IV
RESULTS AND DISCUSSION

4.1 Scallop Surface

Plaster of Paris in the test section was photographed every 30 minutes for five hours to observe the formation of scallops.

4.1.1 The Effect of pH (Defect-Free Plaster)

The effect of pH was observed every 30 minutes for 5 hours at two different flow rates (25 and 35 LPM), three different pHs (3, 7 and 10) and a temperature of 30°C. The pH was adjusted by using sodium hydroxide (NaOH) or sulfuric acid (H_2SO_4).

At pH3 and the low flow rate (25LPM), scallops initiated within the first 30 minutes and the population of scallops increased with time. It is shown that runs at pH3 (Figure 4.1 from a1 to a5) resulted in a larger population of scallops spread randomly on the plaster surface than runs at pH7 and 10. Moreover, the flow rate had an effect on size, shape and possibly the population of scallops on the plaster surface. The average size of scallops was found to decrease with increasing flow rate. At pH3 and the high flow rate (35LPM), scallops also initiated within the first 30 minutes and the populations increased with time. The populations of scallops were similar at pH7 and pH10, and were randomly spread on the plaster surface. Consequently, it can be concluded that flow rate affects the scallop initiation more significantly than pH.

At pH7 and pH10, the results were similar to those at pH3 (Figure 4.2 b1 to b5, and c1 to c5); the scallops initiated within 30 minutes either at low flow rate or high flow rate.

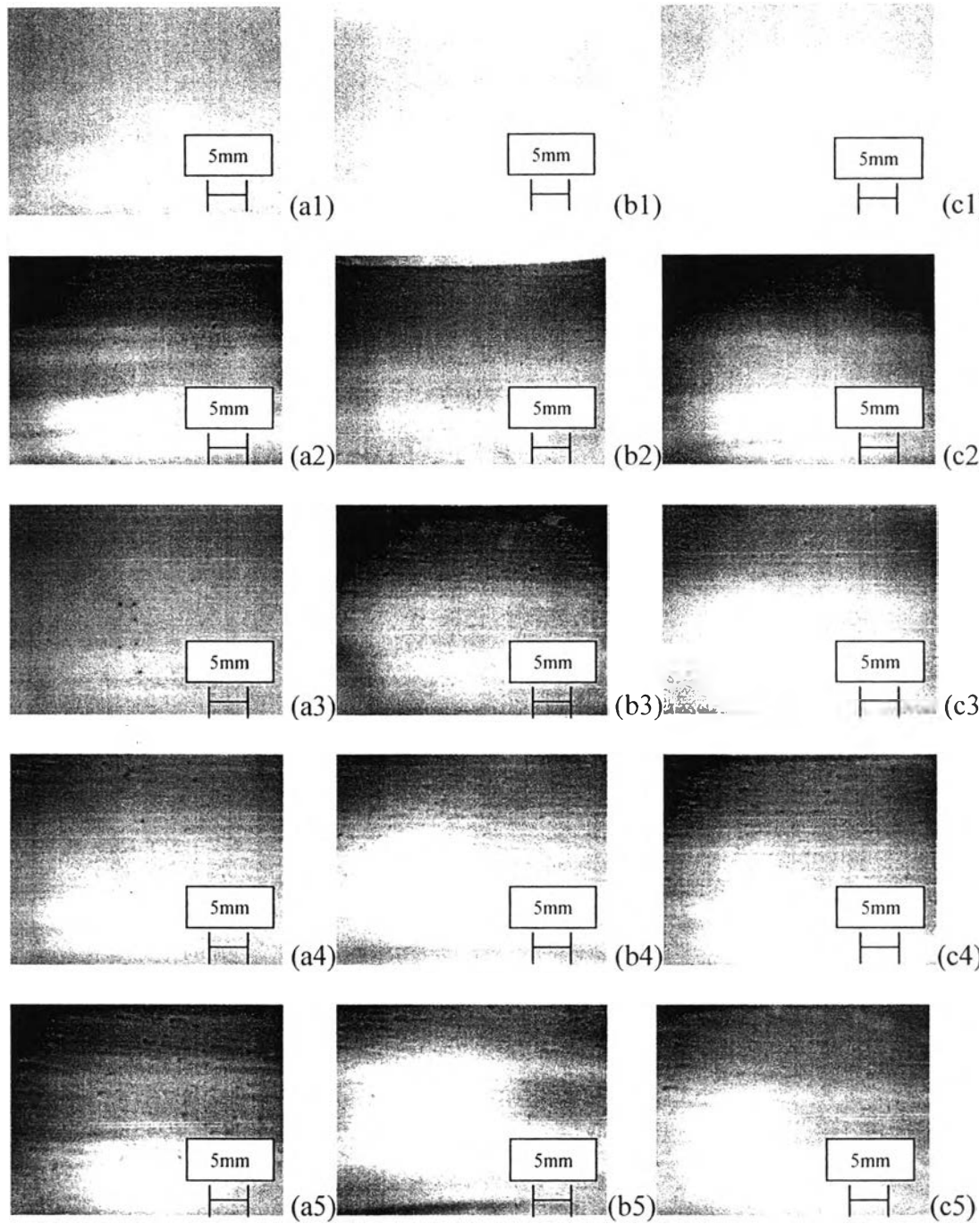

Figure 4.1 Scallop formation on defect-free plaster suface every hour at different pHs, 25 LPM and 30°C: (a1) – (a5) run at pH3, (b1) – (b5) run at pH7, (c1) – (c5) run at pH10.

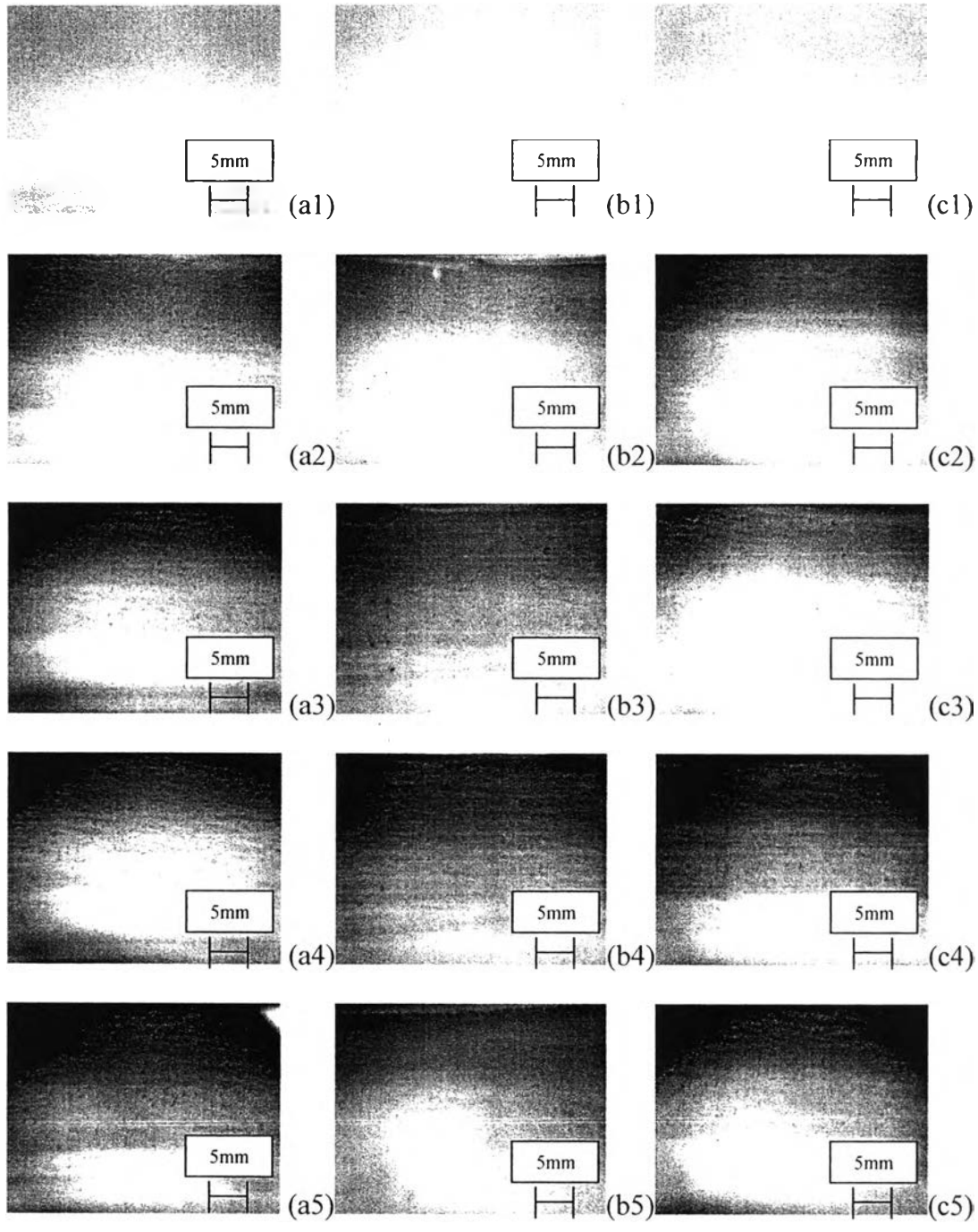

Figure 4.2 Scallop formation on defect-free plaster suface every hour at different pHs, 35 LPM and 30°C: (a1) – (a5) run at pH3, (b1) – (b5) run at pH7, (c1) – (c5) run at pH10.

4.1.2 The Effect of Flowrate

Plaster surfaces with no defects at water flow rates of 25 LPM and 35 LPM indicated that there was different scalloping. At 25 LPM, scallops spread randomly over the surface and seemed to be larger than at the high flow rate, while at 35 LPM there was a large population of small scallops, as shown in Figure 4.3. The average size of scallops was found to decrease with increasing water flow rate because more scallops overlapped. It can be concluded that the population of scallops was observed to develop significantly faster with increasing fluid flow rate (as higher Reynolds number or higher turbulence occurred at the same time), whereas the average size of the scallops was found to decrease. It can be concluded that different flow rates cause different scallops.

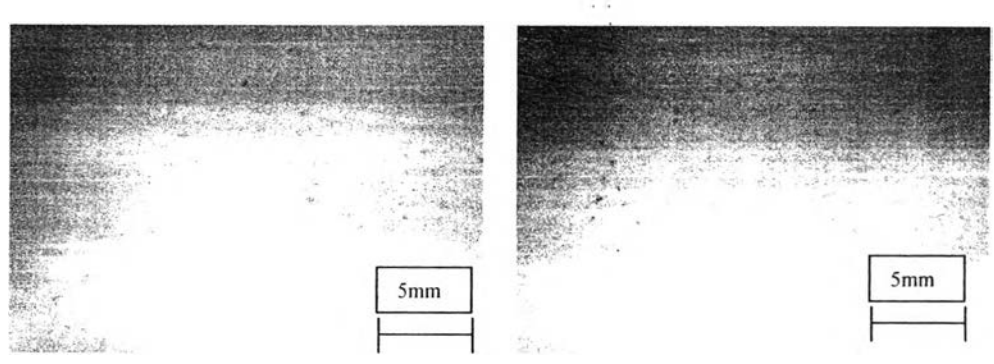

(a) (b)

Figure 4.3 Scallop formation on defect-free plaster surface at different flow rates at pH 7, 30°C: (a) 25 LPM (b) 35LPM.

4.1.3 The Effect of Initial Presence of Defects

Plaster of Paris was mixed with sand grains of different sizes and different concentrations to investigate the effect of initial presence of defects. All runs were operated under different sizes of sand grains (0.21 – 0.25mm, 0.42 – 0.50mm and 0.500 – 0.707mm), defect concentrations (50 and 100 defects/cm^3 of plaster), temperatures (10°C and 25°C) and flow rates (25LPM and 35LPM).

4.1.3.1 Effect of Particle Size

Different sizes of sand grains were added during the mixing of the plaster. Three different grain sizes were used with diameters of 0.21-0.25mm, 0.42-0.50mm and 0.500-0.707mm. Experiments were run at flow rates of 25LPM and 35 LPM, temperatures of 10°C and 25°C. Defect concentrations were adjusted to be 50 defects/cm^3 and 100 defects/cm^3.

Plaster of Paris in the test section was photographed to observe the effect of particle size on the scallop formation. Figure 4.4 shows the size of scallops initiated from different sizes of initial defects. It shows that size of scallops increases with increasing sand size; this supports the Defect theory.

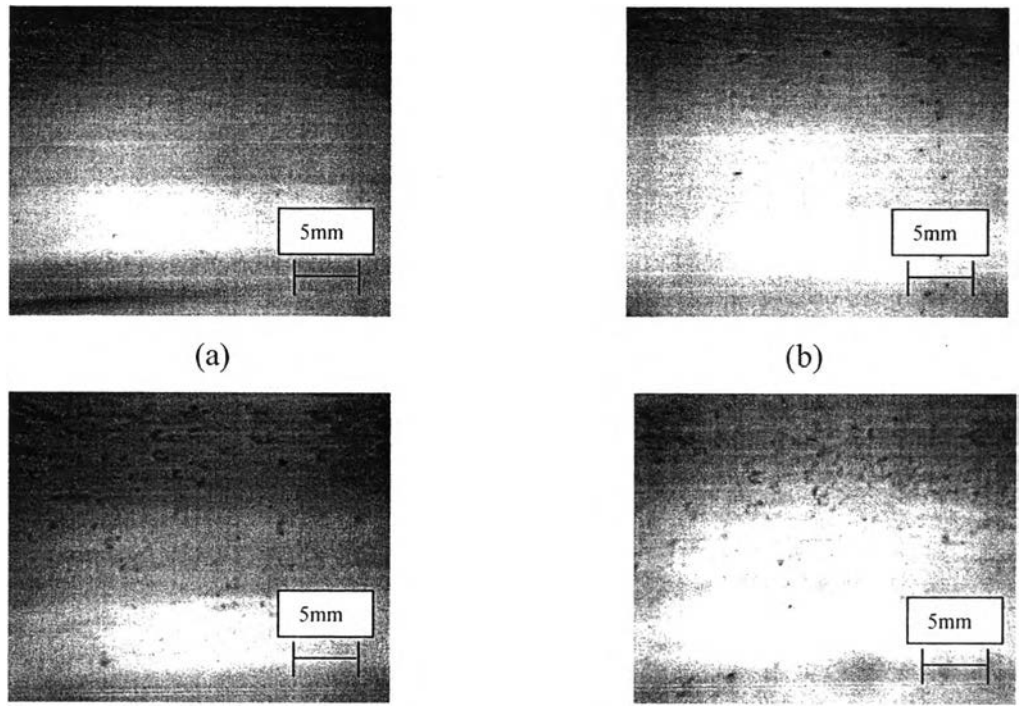

Figure 4.4 Scallop formation on plaster suface at different sizes of initial defects at 25°C, 25LPM and 50 defects/cm^3: (a) pure plaster (b) 0.21-0.25mm (c) 0.42-0.50mm and (d) 0.505-0.707mm.

4.1.3.2 Effect of Defect Concentration

Plaster of Paris was mixed with sand at different defect concentrations. Since the dispersion of sand grains on the surface (defects/cm^2) is difficult to obtain uniformly, the sand concentration (defects/cm^3) was vary used.

Plaster of Paris was mixed with sand at different defect concentrations. Since the dispersion of sand grains on the surface (defects/cm^2) is difficult to obtain uniformly, the sand concentration (defects/cm^3) was vary used.

Different concentrations of initial defects present different scalloping surfaces. As shown in Figure 4.5, it seems that populations of scallops increase with increasing concentration of initial defects. A defect size of 0.500-0.707 mm, 25 LPM and 25°C, population of scallops at 50 defects/cm^3 is lower than population of scallops at 100 defects/cm^3. This supports the Defect theory.

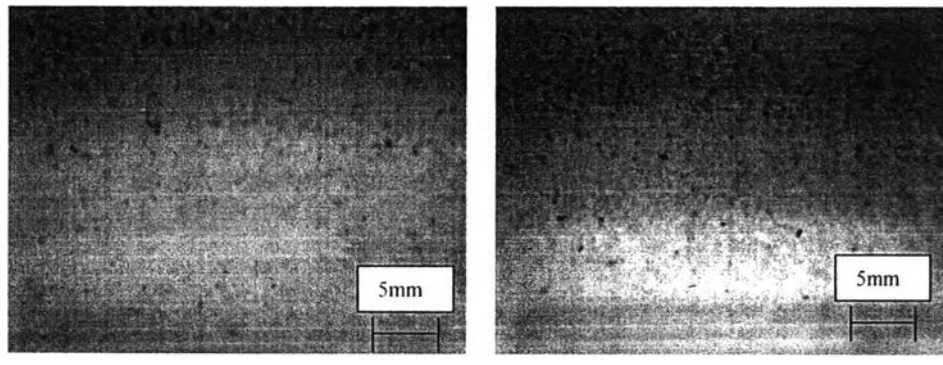

(a) (b)

Figure 4.5 Scallop formation on plaster suface at different concentrations of initial defects at 25°C, 25LPM. 0.500-0.707 mm: (a) 50 defects/cm^3 (b) 100 defects/cm^3.

4.1.4 The Effect of Temperature

Experiments were performed at different temperatures (10°C and 25°C). Plaster of Paris was mixed with the sand grains at different sizes and different concentration to observe the effect of the initial presence of defects. Tests were conducted under different sizes of sand grains (0.21 – 0.25mm, 0.420 – 0.50mm and 0.500 – 0.707mm), defect concentrations (50 and 100 defects/cm^3 of plaster) and flow rates (25LPM and 35LPM).

The plaster of Paris in the test section was photographed to observe the effect of temperature on scallop formation. Figure 4.6 shows a comparison of the population of scallops between low and high temeratures. It shows that the population of scallops decreases with decreasing temperature.

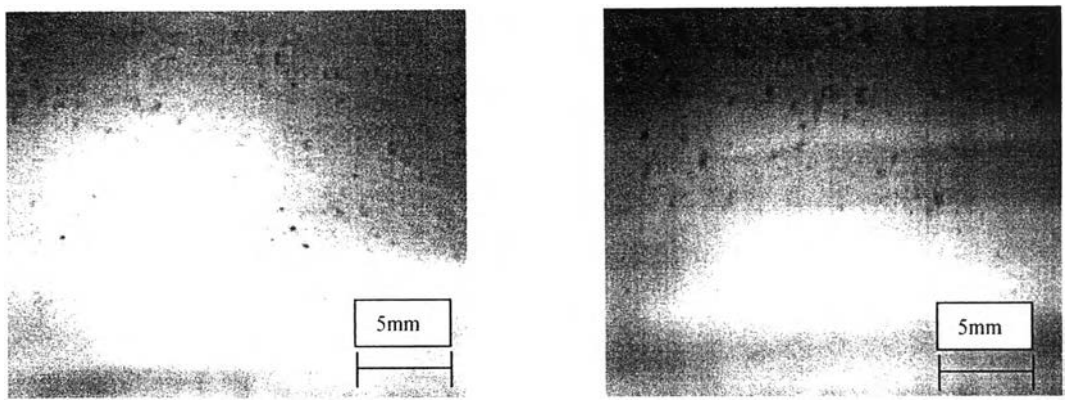

(a) (b)

Figure 4.6 Scallop formation on plaster suface at different temperatures at 25LPM, 0.42-0.50 mm and 50 defects/cm^3: (a) 25°C (b) 10 °C.

4.2 Dissolution Rate

The dissolution rate was determined in two ways; the dissolution rate with time and the dissolution rate along the pipe length. The dissolution rate with time was observed every 30 minutes for five hours by measuring Ca^{2+} by AAS. The dissolution rate along the pipe length was obtain by measuring the thickness of the pipe after five-hour experiment. The experiments were run at different pHs (pH3, 7 and 10), flow rates (25LPM and 35LPM) and a temperature of 30°C.

4.2.1 Dissolution Rate with Time

4.2.1.1 The Effect of pH

At 25 LPM, as shown in Figure 4.67, after 120 minutes, all pHs were found to show similar results. The dissolution rate of plaster increased at 60 minutes possibly because of the initiation of scallops. The formation of scallops causes the surface area of plaster to increase with time. Consequently, the dissolution rate also increased with time. Another possibility is the plaster was more dried so it was easily dissolved into the bulk within 30 minutes. The results correspond to those of Shao (2006); he found that scallops developed rapidly at the beginning of the test, which corresponded to an increase of water conductivity. He suggested that a higher

reduced when the dissolution of plaster of Paris increased the Ca^{2+} and SO_4^{2-} ion concentrations in a re-circulating system.

In the pH3 runs at 25LPM, the dissolution rate increased until 150 minutes because of the increasing of populations of scallops and surface area; hence, dissolution rate increased. It then became stable but started to increase again after 240 minutes. pH7 at 25 LPM shows similar results to pH3; the dissolution rate increased until 180 minutes. It then dropped and started to increase again after 270 minutes.

pH10 runs at 25LPM also showed similar results to those of pH3 and pH7 within the first 120 minutes but gave a higher dissolution rate. After 120 minutes, the dissolution rate starts to decrease instead of the increase expected from the increasing surface area of plaster. Therefore, some phenomenon had more effect on the dissolution rate than the increasing of surface area.

Chemical reaction on the plaster surface was the first possibility to be taken into account. Water with sodium hydroxide was used to run through the test section at pH10, so calcium hydroxide was formed and deposited on the plaster surface. The plaster surface may be coated with the calcium hydroxide and the solubility of calcium decreases with the increasing alkaline solution (solubility of calcium sulfate is higher than that of calcium hydroxide (W.Rechenberg and S.Sprung, 1983)). Hence, calcium hydroxide deposited and coated the plaster surface and the solubility of plaster decreased.

$$CaSO_4 + NaOH \longrightarrow Ca(OH)_2 + Na_2SO_4$$

Precipitated

Berger *et al.*,(1977) mentioned that increasing the sodium hydroxide concentration in the solution will lead to a lower diffusion coefficient. From Figure 4.7 shows that the dissolution rate, at pH10, decreases with time. This suggests that calcium hydroxide had slowly coated on the plaster surface.

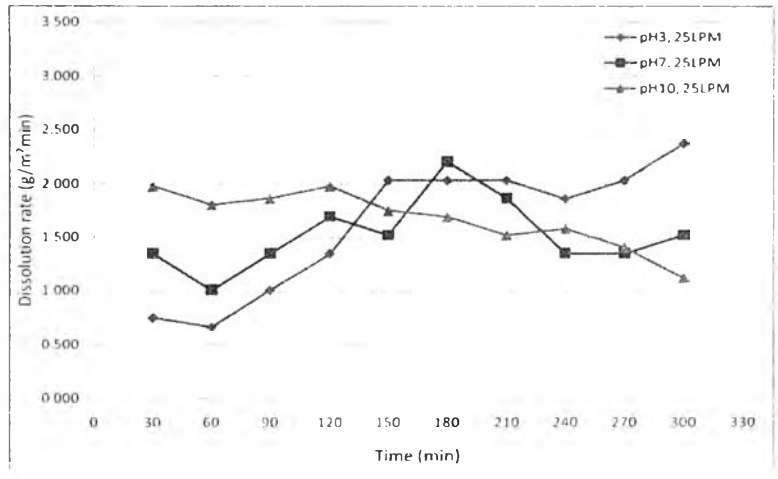

Figure 4.7 The effect of pH on the dissolution rate of plaster with time, 25LPM, 30°C.

The average dissolution at each pH was similar. These results correspond to the results of G.Azimi *et al.*,(2007) and W.Rochenberg and S.Sprung (1982). Table 4.1 shows the average dissolution rate for 300 minutes. The results show that all pHs have a similar average dissolution rate. The average dissolution rate at 25LPM, pH3 is higher than at pH7 but less than at pH10. This means at pH10, plaster dissolves at the highest rate of dissolution for the 300 minute test. The data indicate that pH does not have a significant effect on the dissolution rate of gypsum.

The average dissolution at each pH was similar. These results correspond to the results of G.Azimi *et al.*,(2007) and W.Rochenberg and S.Sprung (1982). Table 4.1 shows the average dissolution rate for 300 minutes. The results show that all pHs have a similar average dissolution rate. The average dissolution rate at 25LPM, pH3 is higher than at pH7 but less than at pH10. This means at pH10, plaster dissolves at the highest rate of dissolution for the 300 minute test. The data indicate that pH does not have a significant effect on the dissolution rate of gypsum.

Table 4.1 Average dissolution rate calculated from AAS at different pHs and 25LPM.

Time (min)	pH3	pH7	pH10
30	0.764	1.458	1.98
60	0.679	1.418	1.81
90	1.018	1.658	1.866
120	1.358	1.697	1.98
150	2.036	1.527	1.753
180	2.036	2.206	1.697
210	2.036	1.867	1.527
240	1.867	1.458	1.584
270	2.036	1.458	1.414
300	2.376	1.527	1.131
Average dissolution rate (g/m^2min)	1.621	1.6274	1.674

The dissolution rate at 35LPM shows similar trends to the dissolution rate at 25LPM. The dissolution rates at pH3 and pH7 tend to increase with time. On the other hand, the dissolution rate at pH10 decreases with time.However, because of the scatter of the measurements, these trends may not be significant (see Figure 4.8).

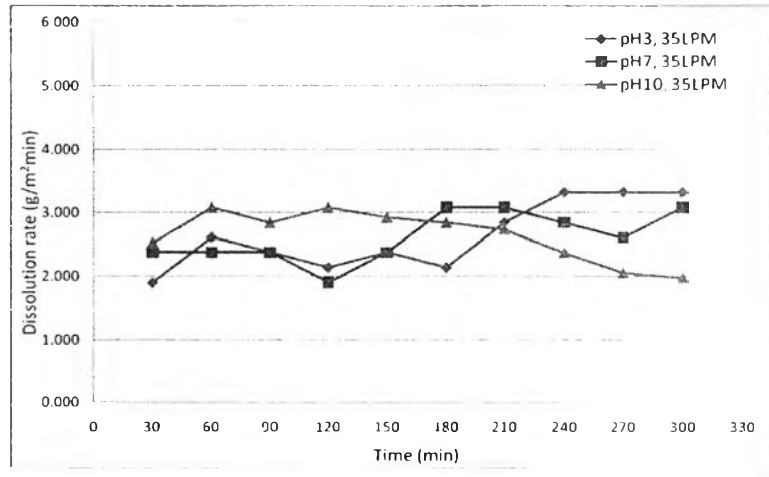

Figure 4.8 The effect of pH on the dissolution rate of plaster of Paris with time at 35LPM, 30°C.

Table 4.2 shows the average dissolution rate at the high flowrate, the trends are similar to those at the low flowrate but the rates are higher. The average dissolution rate at pH3 is higher than the average dissolution rate at pH7 but less than at pH10. This again indicates that pH does not have a significant effect on dissolution rate of gypsum.

Table 4.2 Average dissolution rate calculated from AAS at different pHs and 35 LPM.

Time (min)	pH3	pH7	pH10
30	1.901	2.376	2.534
60	2.613	2.376	3.088
90	2.376	2.376	2.851
120	2.138	1.901	3.088
150	2.376	2.376	2.930
180	2.138	3.088	2.851
210	2.851	3.088	2.748
240	3.326	2.851	2.376
270	3.326	2.613	2.059
300	3.326	3.088	1.980
Average dissolution rate (g/m^2min)	2.637	2.613	2.651

4.2.1.2 The Effect of Flow Rate

The dissolution rate with time increases with increasing flow rate (see Appendix A1.1). As the process continues, scallops initiate on the plaster surface. The formation of scallops causes the surface area of plaster to increase with time and also causes the dissolution rate to increase with time as shown in Figure 4.9. A higher flow rate will cause a higher dissolution rate.

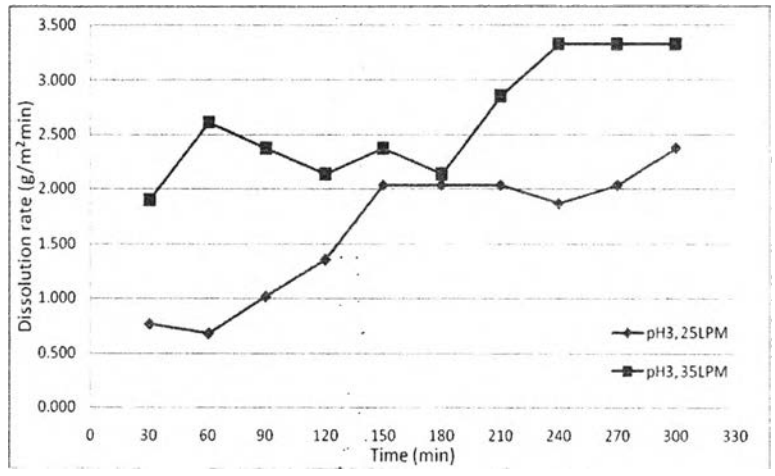

Figure 4.9 Effect of flow rate on the dissolution rate with time at pH3 and 30°C.

4.2.1.3 The Effect of Particle Size

From Figures 4.10 and 4.11, the dissolution rate of plaster with defects with time shows fluctuating results. This may because of the dispersion of sand grains. The sand may not disperse uniformly and homogeneously on the suface causing uneven detachment of sand grains and uneven formation of scallops. As a result, the plaster dissolves unevenly with time. Pure plaster presents the least uneven dissolution rates. This supports the idea that the uneven dissolution rate araises from the effect of dispersion of sand particles.

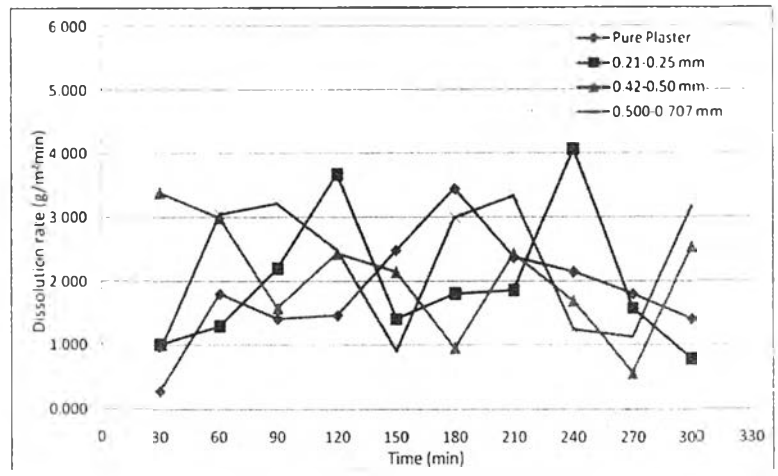

Figure 4.10 Dissolution rate with time at different sizes of particles, 25°C, 50 defects/cm^3 and 25LPM.

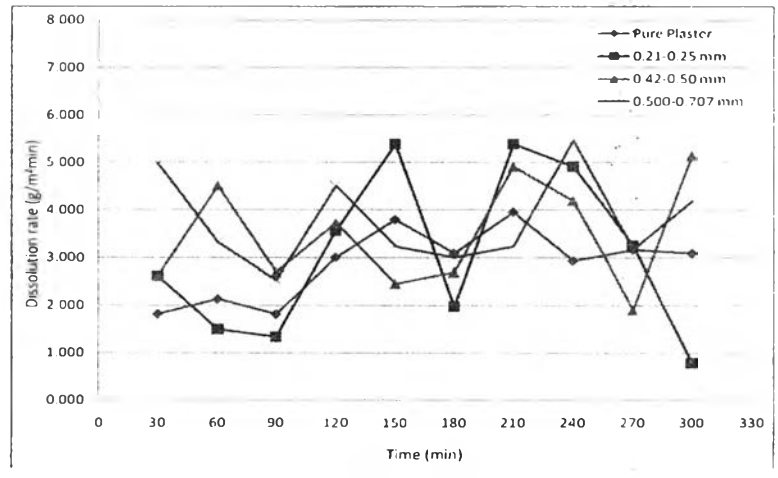

Figure 4.11 Dissolution rate with time at different sizes of particles, 25°C, 50 defects/cm^3 and 35LPM.

The average dissolution rate was determined to yield the effect of particle size on the dissolution rate with time. Size of particles has a significant effect on the dissolution rate with time. Larger size particles give larger scallops, causing a larger surface area and a higher rate of dissolution. As a result, the dissolution rate increases with increasing particle size. As shown in Tables 4.3 and 4.4, the largest

defects (0.500-0.707 mm) give the highest average rate of dissolution and pure plaster gives the lowest rate of dissolution (see Appendix A.1.2).

Table 4.3 Average dissolution rate calculated from AAS at different sizes of initial defects and 25 LPM and 25°C.

Time (min)	Pure Plaster	0.21-0.25 mm 50 defects/cm^3	0.42-0.50 mm 50 defects/cm^3	0.500-0.707 mm 50 defects/cm^3
30	0.283	1.018	3.394	0.905
60	1.810	1.301	2.998	3.055
90	1.414	2.206	1.584	3.224
120	1.471	3.677	2.432	2.489
150	2.489	1.414	2.149	0.905
180	3.451	1.810	0.962	2.998
210	2.376	1.867	2.432	3.337
240	2.149	4.073	1.697	1.244
270	1.810	1.584	0.566	1.131
300	1.414	0.792	2.545	3.168
Average dissolution rate (g/m^{2}min)	1.867	1.974	2.076	2.246

Table 4.4 Average dissolution rate calculated from AAS at different sizes of initial defects and 35 LPM and 25°C.

Time (min)	Pure Plaster	0.21-0.25 mm 50 defects/cm^3	0.42-0.50 mm 50 defects/cm^3	0.500-0.707 mm 50 defects/cm^3
30	1.821	2.613	2.613	4.989
60	2.138	1.505	4.514	3.326
90	1.821	1.346	2.693	2.534
120	3.009	3.564	3.722	4.514
150	3.801	5.543	2.455	3.247
180	3.088	1.980	2.693	3.009
210	3.960	5.860	4.910	3.247
240	2.930	4.910	4.197	5.464
270	3.168	3.247	1.901	3.168
300	3.088	0.792	5.147	4.197
Average dissolution rate (g/m^{2}min)	2.883	3.136	3.484	3.770

4.1.4 The Effect of Particle Concentration

From Figures 4.12 and 4.13, the dissolution rate with time shows uneven behavior. This maybe because of the dispersion of sand grains. Sand might not disperse uniformly and homogeneously on the suface causing uneven detachment of sand grains and uneven formation of scallops. As a result, the plaster dissolves unevenly causing a variation in dissolution rate. The pure plaster gives the least uneven dissolution rate. This supports the theory that the variation of the dissolution rate is caused by the uneven dispersion of sand particles.

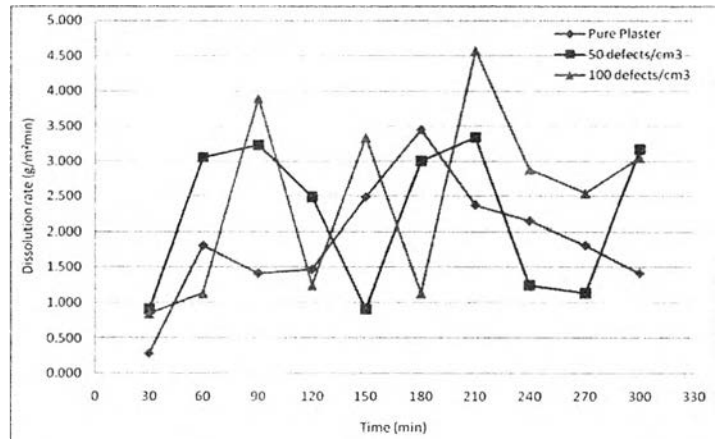

Figure 4.12 Dissolution rate with time at different concentrations of particles, 0.500-0.707 mm, 25°C and 25LPM.

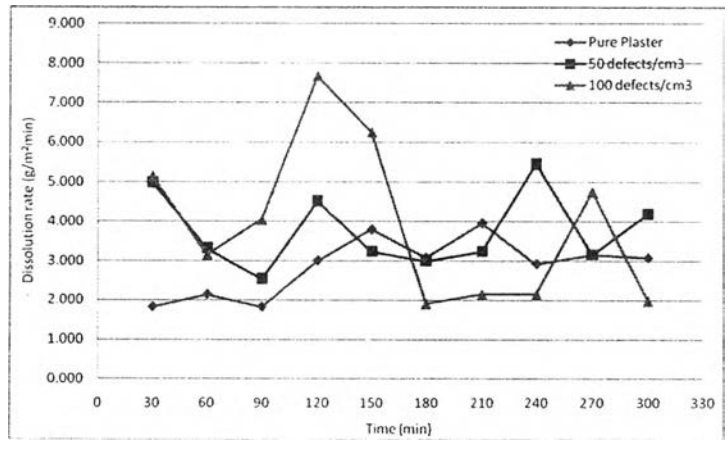

Figure 4.13 Dissolution rate with time at different concentrations of particles, 0.500-0.707 mm, 25°C and 35LPM.

The average dissolution rate was determined to indicate the effect of particle concentration on the dissolution rate with time. The concentration of particles has a significant effect on the dissolution rate with time. The higher amount of particles gives a larger number of scallops, causing larger surface area and a higher rate of dissolution. As a result, dissolution rate increases with increasing particle concentration. As shown in Table 4.5 and 4.6, the defect concentration of 100 defects/cm^3 gives a higher average dissolution and pure plaster gives the lowest total dissolution (see Appendix A.1.3).

Table 4.5 Average dissolution rate calculated from AAS at different concentrations of initial defects at defect size of 0.500-0.707 mm, 25LPM and 25°C.

Time (min)	Pure plaster	0.500-0.707 mm 50 defects/cm^3	0.500-0.707 mm 100 defects/cm^3
30	0.283	0.905	0.848
60	1.810	3.055	1.131
90	1.414	3.224	3.903
120	1.471	2.489	1.244
150	2.489	0.905	3.337
180	3.451	2.998	1.131
210	2.376	3.337	4.582
240	2.149	1.244	2.885
270	1.810	1.131	2.545
300	1.414	3.168	3.055
Average dissolution rate (g/m^{2}min)	1.867	2.246	2.466

Table 4.6 Average dissolution rate calculated from AAS at different concentrations of initial defects at defect size of 0.500-0.707 mm and 35LPM and 25°C.

Time (min)	Pure Plaster	0.500-0.707 mm 50 defects/cm^3	0.500-0.707 mm 100 defects/cm^3
30	1.821	4.989	5.147
60	2.138	5.464	3.168
90	1.821	2.534	4.039
120	3.009	3.168	7.682
150	3.801	3.247	6.256
180	3.088	3.009	1.901
210	3.960	3.247	2.138
240	2.930	3.326	2.138
270	3.168	4.514	4.752
300	3.088	4.197	1.980
Average dissolution rate (g/m^{2}min)	2.883	3.770	3.920

4.2.1.5 The Effect of Temperature

The dissolution rate vs time at the higher temperature gives a higher rate than at the lower temperature (see Appendix A.1.4). Since the population of scallops increases with temperature, the dissolution rate also increases with increasing temperature. Results from Azimi *et al,* 2007, determined the solubility of plaster at different temperatures and found a decrease of 7.19% between 25°C to 10°C. The dissolution rate at high temperature is more uneven than at low temperature. The uneven dissolution rate maybe caused by the effect of additional sand grains. However, the low temperature shows less variation than the high temperature.

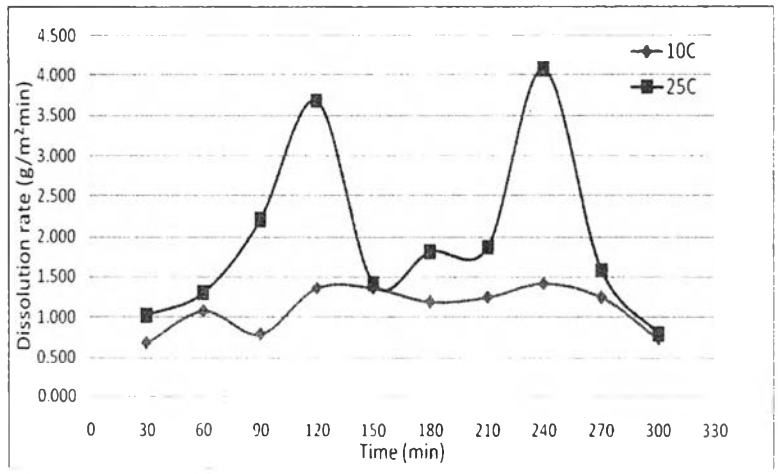

Figure 4.14 Dissolution rate with time at different temperatures , 0.21-0.25 mm, 50 defects/cm^3 and 25LPM.

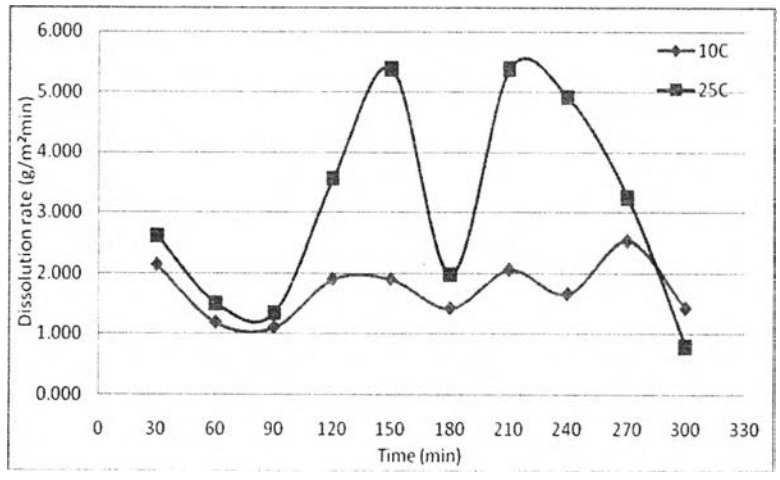

Figure 4.15 Dissolution rate with time at different temperatures , 0.21-0.25 mm, 50 defects/cm^3 and 35LPM.

4.2.2 Dissolution Rate along the Pipe Length

The dissolution rate along the pipe was obtained at the end of an experiment by measuring the thickness at three circumferential points every centimeter along the plaster pipe, and converting these measurements into dissolution rate.

4.2.2.1 The Effect of pH

Dissolution rates along the pipe at different pHs for plaster with no defects are shown in Figure 4.16 and Figure 4.17. The dissolution rates show the same trends at different pHs. This indicates that pH has essentially no effect on the dissolution rate along the pipe length. The results show the dissolution rate is much higher at the inlet of the pipe (first few centimeters) and then substantially decreases and gradually decreases along the pipe length. This may due to non uniform and highly turbulent flow at the connection between the main pipe and the test section causing a much higher dissolution rate. The remainder of dissolution rate along the pipe shows the small fluctuations.

The low flow rate (25LPM) shows a greater decreases in dissolution rate at the entrance than the high flow rate. The average rates along the pipe length correspond very well with those measured on-time by AAS (see Tables 4.1 and 4.2).

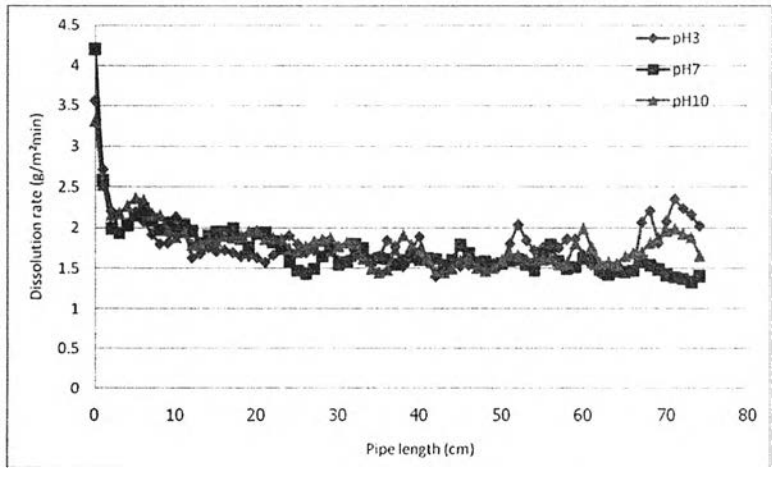

Figure 4.16 Dissolution rate along the pipe at 25LPM, 30°C.

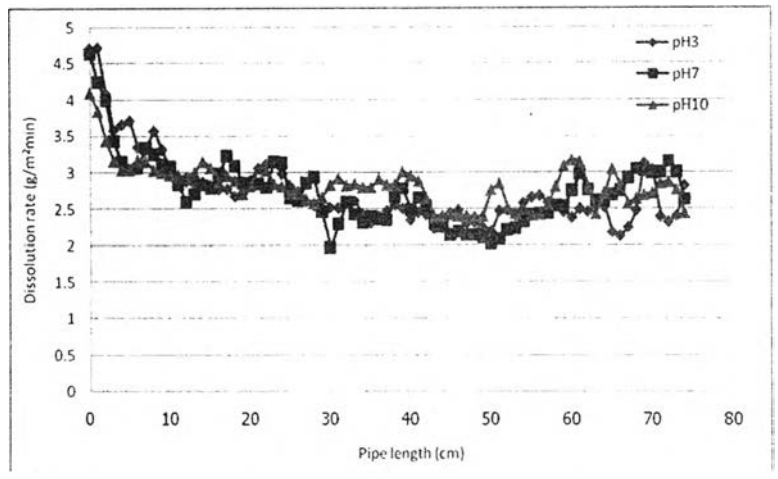

Figure 4.17 Dissolution rate along the pipe at 35LPM, 30°C.

From the different results of the inlet effect as shown above, the conduit was photographed at the entrance and the exit to compare between low and high flow rates – see Figure 4.18. It was found that the entrance of a conduit has a thinner wall than the exit. The connection between the main pipe and the test section causes a more disturbed flow at the entrance. This causes higher turbulence and a higher dissolution rate near the entrance. At low flow rate, the thickness at the entrance of the conduit is approximately half that of the outlet. On the other hand, the thickness of the pipe seems to be similar along the length at high flow rate.

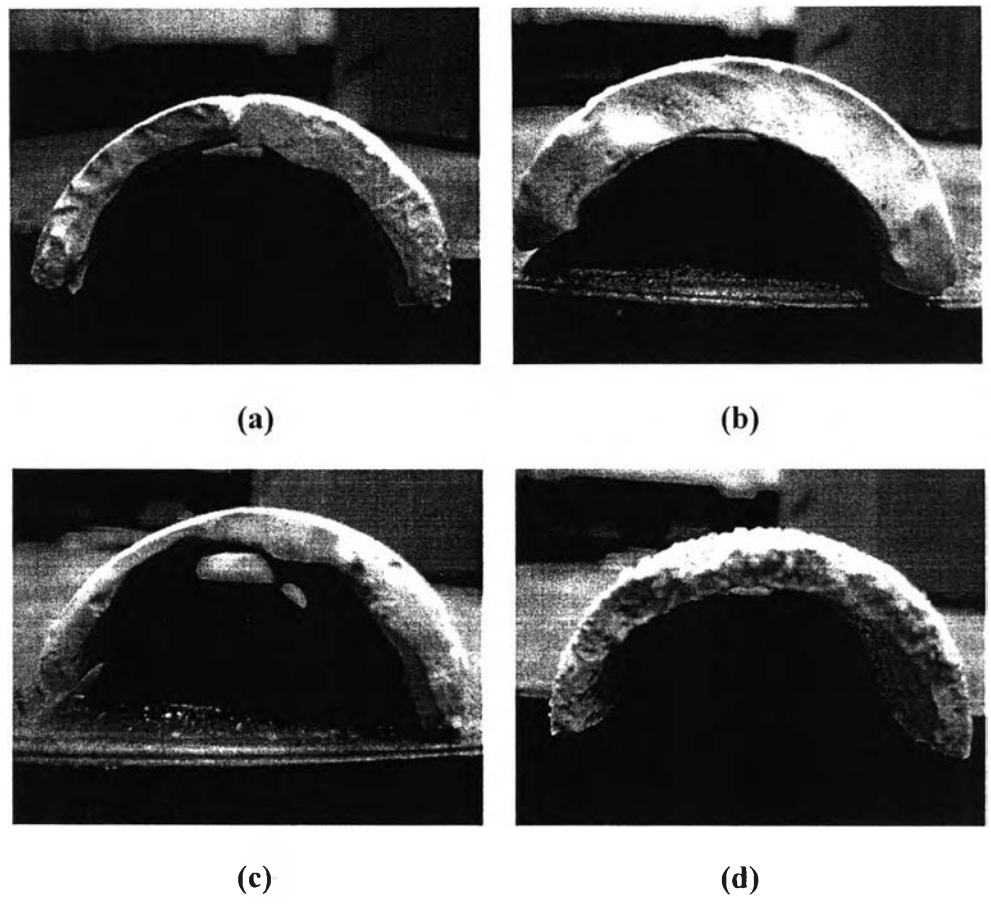

Figure 4.18 Plaster test section at different positions (a) 25 LPM at the entrance, (b) 25 LPM at the exit, (c) 35 LPM at the entrance, (d) 35 LPM at the exit.

Table 4.7 shows the average dissolution rate calculated from thickness of plaster at three circumferential points every centimeter after the end of the test. The results show that dissolution rate is approximately the same for the three pHs. This confirms that pH does not have a significant effect on the dissolution rate of gypsum. This result corresponds to the average dissolution rate calculated from AAS. This confirms that pH has little effect on dissolution of plaster.

Table 4.7 Average dissolution rate calculated from the thickness of pipe at different pHs and different flowrates.

pH	Flowrate (LPM)	Average dissolution rate (g/m^2min)	Flowrate (LPM)	Average dissolution rate (g/m^2min)
3	25	1.805	35	2.752
7	25	1.832	35	2.747
10	25	1.811	35	2.735

4.2.2.2 The Effect of Flow Rate

Different flow rates give a significant change in the dissolution rate or erosion of the plaster pipe. A higher flow rate dissolves more plaster into the bulk water. Figure 4.19 shows a strong effect of flow rate on dissolution of plaster. pH3, pH7 and pH10 show a similar result for the effect of flow rate on the dissolution of plaster (see Appendix A.2.1).

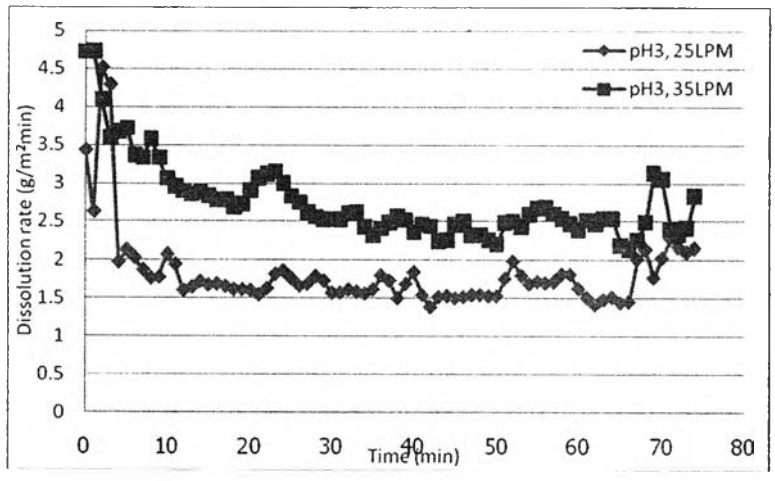

Figure 4.19 Dissolution rate along the pipe length at pH3 and 30°C.

4.2.2.3 The Effect of Particle Size

Figures 4.20 and 4.21 show the dissolution rate along the pipe length. It shows that the largest particles give a higher rate of dissolution along the pipe length (see Appendix A.2.2). As mentioned above, larger particles give larger

scallops. Moreover, roughness on the surface interacts with the laminar sublayer. If the size of roughness is greater than the thickness of the laminar sublayer then it increases the disturbance in the flow. This leads to a larger surface area and a higher rate of dissolution. As a result, the dissolution rate increases with increasing particle size. The largest size of particle (0.500 – 0.707 mm) gives the highest rate of dissolution and pure plaster gives the lowest rate. The effect of turbulent flow still has an effect on the dissolution at the inlet of pipe. This causes a higher dissolution rate at the entrance.

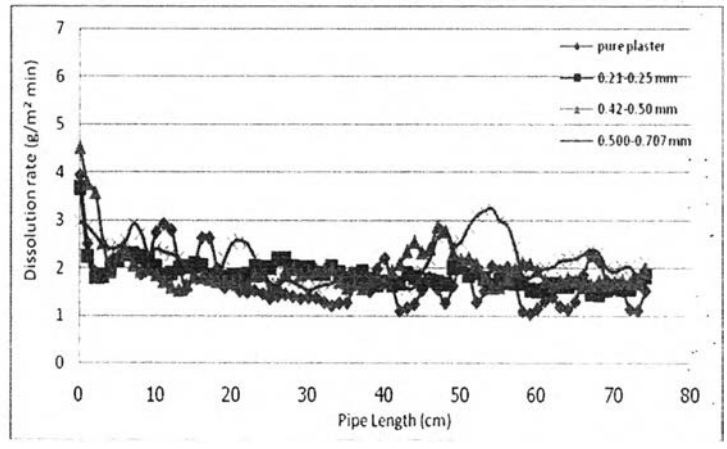

Figure 4.20 Dissolution rate along the pipe at different particle sizes, 50 defects/cm^3, 25LPM and 25°C.

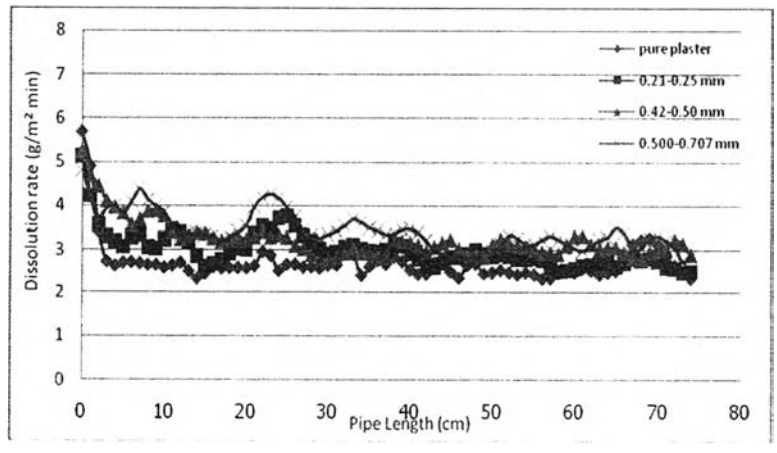

Figure 4.21 Dissolution rate along the pipe at different particle sizes, 50 defects/cm^3, 35LPM and 25°C.

Table 4.8 shows the average dissolution rate calculated from thickness of plaster at three points every centimeter at the end of the test (see Appendix A.2.2). The results show that the average dissolution rate increases with increasing size of initial defects. This result corresponds to the average dissolution rate calculting from AAS.

Table 4.8 Average dissolution rate calculating from the thickness of pipe at different sizes of initial defects and different flowrates.

Defect Size (mm)	Defect concentration (defects/cm^3)	Flowrate (LPM)	Average dissolution rate (g/m^{2}min)	Flowrate (LPM)	Average dissolution rate (g/m^{2}min)
Pure plaster	50	25	1.729	35	2.709
0.21-0.25	50	25	1.875	35	2.991
0.42-0.50	50	25	1.985	35	3.240
0.500-0.707	50	25	2.181	35	3.425

4.2.2.4 The Effect of Particle Concentration

Figures 4.22 and 4.23 show the dissolution rate along the pipe length for different defect concentrations. The figures indicate that the greater number of particles give the higher rate of dissolution along the pipe length (see Appendix A.2.3). As mentioned above, a greater number of particles gives larger amounts of scallops, causing a larger surface area and a higher rate of dissolution. This means the dissolution rate increases with increasing particle concentration. The greater number of particles (100 defects/cm^3) give the higher rate of dissolution and pure plaster gives the lowest rate. The effect of turbulent flow affects the dissolution at the inlet of the pipe. This causes the higher dissolution rate at the inlet.

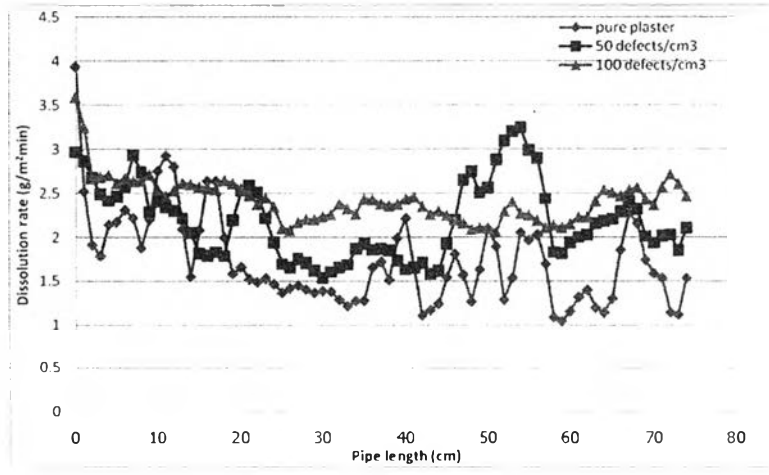

Figure 4.22 Dissolution rate along the pipe at different particle concentrations, 0.500-0.707 mm, 25LPM and 25°C.

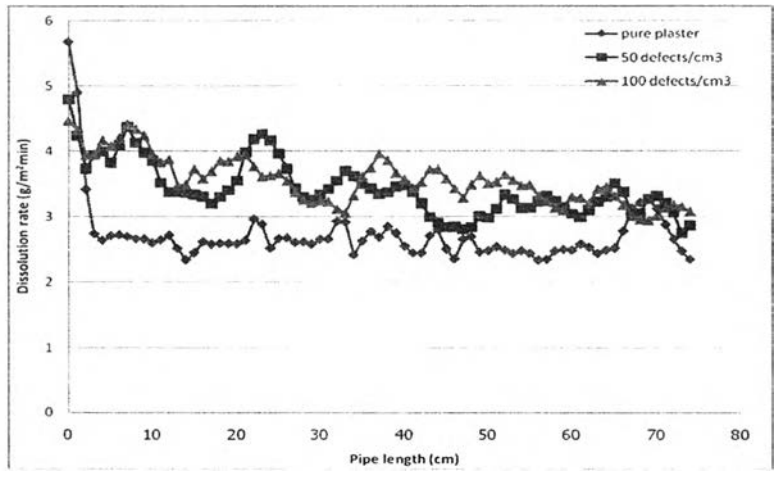

Figure 4.23 Dissolution rate along the pipe at different particle concentrations, 0.500-0.707 mm, 35LPM and 25°C.

Table 4.9 shows the average dissolution rate for plaster with defects calculated from the thickness of plaster at three points every centimeter at the end of the test (see Appendix A.2.3). The results show that the average dissolution rate increases with increasing concentration of initial defects. This result corresponds to the average dissolution rate calculated from AAS.

Table 4.9 Average dissolution rate calculating from the thickness of pipe at different concentrations of initial defects and different flowrates.

Defect concentration (defects/cm^3)	Defect size (mm)	Flowrate (LPM)	Average dissolution rate (g/m^{2}min)	Flowrate (LPM)	Average dissolution rate (g/m^{2}min)
Pure plaster	0	25	1.729	35	2.709
50	0.500-0.707	25	2.181	35	3.425
100	0.500-0.707	25	2.423	35	3.566

4.2.2.5 The Effect of Temperature

Figure 4.24 shows the dissolution rate along the pipe. It shows that the higher temperature gives the higher rate of dissolution along the pipe (see Appendix A.2.4). The dissolution rate is again higher at the entrance.

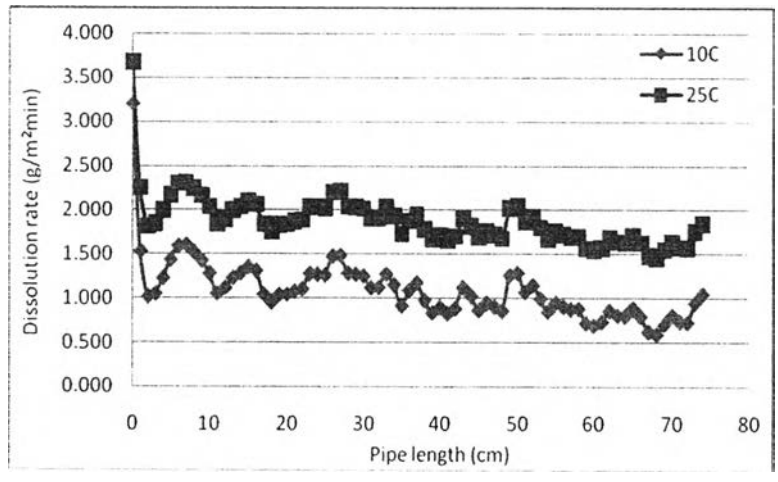

Figure 4.24 Dissolution rate along the pipe at different temperatures, 0.21-0.25 mm, 50 defects/cm^3,25LPM.

4.3 Pressure Drop

Pressure drop was measured by using a differential pressure transducer. Experiments on pressure drop were run at three different values of pH (pH3, 7 and 10), two different flow rates (25LPM and 35 LPM), three different particle sizes (0.21-0.25mm, 0.42-0.50mm and 0.500-0.707mm), two different particle concentrations (50 and 100 defects/cm^3) and two different temperatures (10 and 25°C).

4.3.1 The Effect of pH

The results at low flow rate (25LPM) as shown in Figure 4.25 indicate that pH has no effect on pressure drop. During the experiment, measured pressure drops tend to decrease with time. This is due to an increase in the diameter of the plaster pipe. Since, plaster is continuously dissolving into the bulk liquid, this results in an increase in diameter of the pipe.

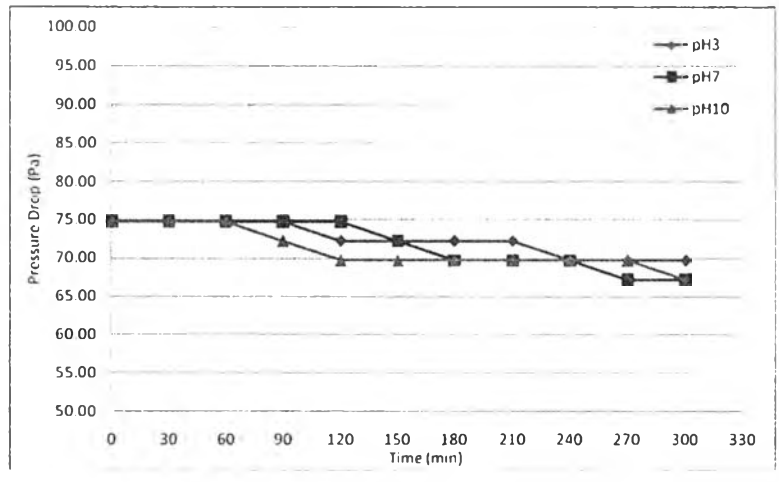

Figure 4.25 Pressure drop with time at 25 LPM, 30°C.

The results at high flow rate (35LPM) as shown in Figure 4.26, also show that pH has no effect on pressure drop. The pressure drops also tend to decrease with time.

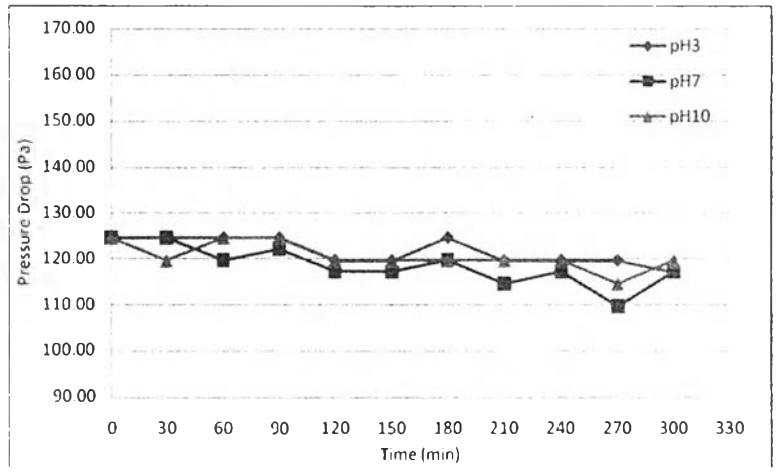

Figure 4.26 Pressure drop with time at 35 LPM, 30°C.

4.3.2 The Effect of Flow Rate

Pressure drop and flow rate are dependent on each other. A higher flow rate, produce a pressure drop. According to the Fanning's equation (see Appendix B.1);

$$P_1 - P_2 = (4f\rho v^2/2)(L_1 - L_2)/D$$

where $P_1 - P_2$ is pressure drop (Pa), f is friction factor, ρ is density of fluid (kg/m^3), V is flow velocity, $L_1 - L_2$ is length of pipe (m) and D is diameter of pipe (m)

Figure 4.27 shows the effect of flow rate on pressure drop for the plaster pipes.

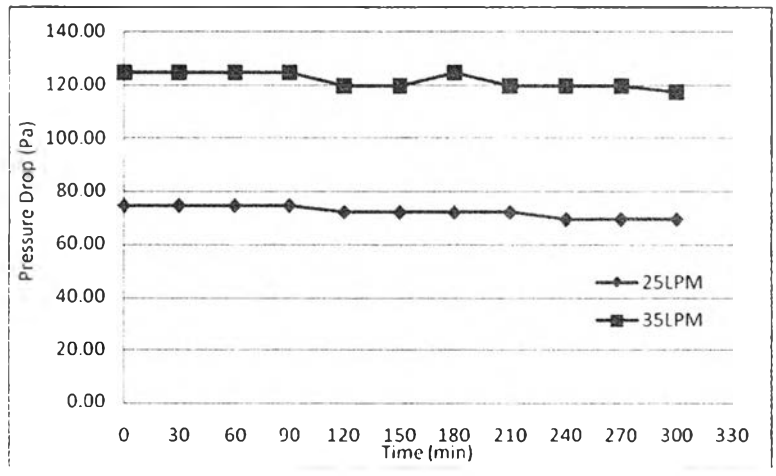

Figure 4.27 Pressure drop with time at pH3, 30°C.

4.3.3 The Effect of Particle Size

There are two opposing effects on the pressure drop which are the effect of roughness and the effect of pipe diameter. Pressure drop will increase with increasing surface roughness whereas it will decrease with increasing pipe diameter. As time passes, plaster is continuously dissolving into the bulk liquid resulting in thinning of the plaster pipe and formation of scallops on the plaster surface causing in increase in diameter and surface roughness, respectively. Figures 4.28 and 4.29 show that pressure drop has decreased with time. This indicates that pipe diameter has a greater effect than surface roughness. The pressure drop at the high flow rate also tends to decrease with time.

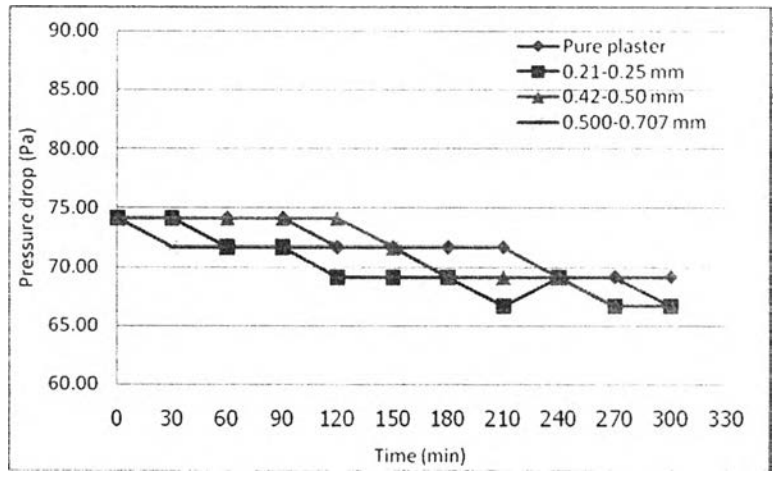

Figure 4.28 Pressure drop at different sizes of particles, 50 defects/cm^3, 25°C and 25LPM.

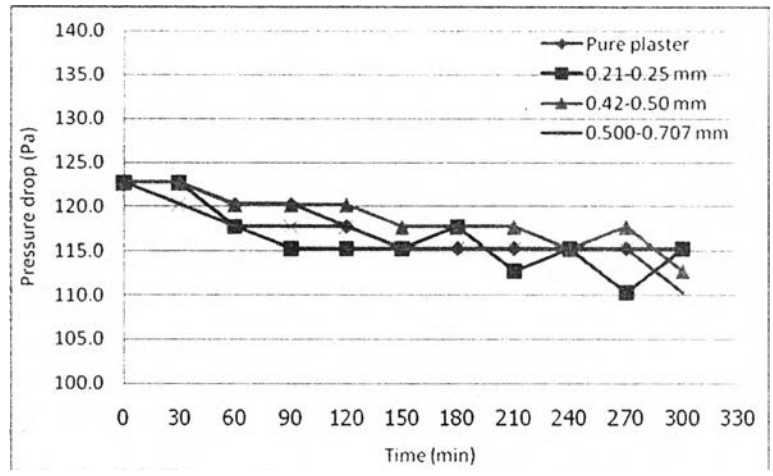

Figure 4.29 Pressure drop at different sizes of particles, 50 defects/cm^3, 25°C and 35 LPM.

4.3.4 The Effect of Particle Concentration

Figures 4.30 and 4.31 show that the pressure drop decreased with time. This confirms that the diameter of pipe has a greater effect than the surface roughness. Pressure drop at high flow rate also tends to decrease with time.

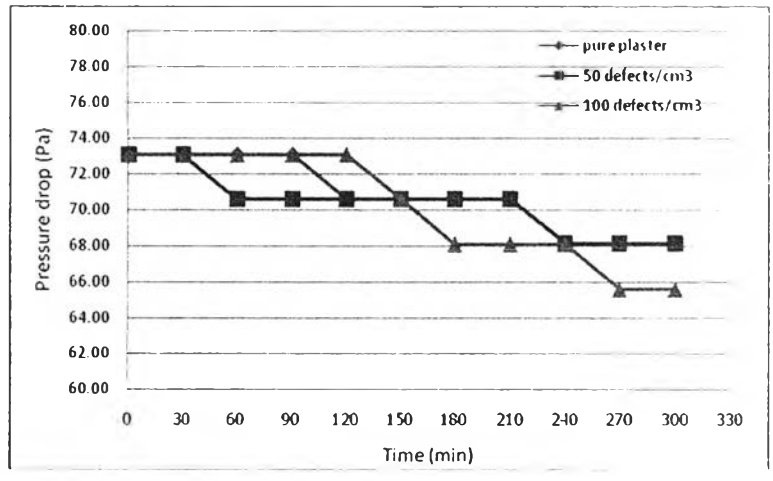

Figure 4.30 Pressure drop with time at different concentrations of particles, 0.42-0.50 mm, 25°C and 25 LPM.

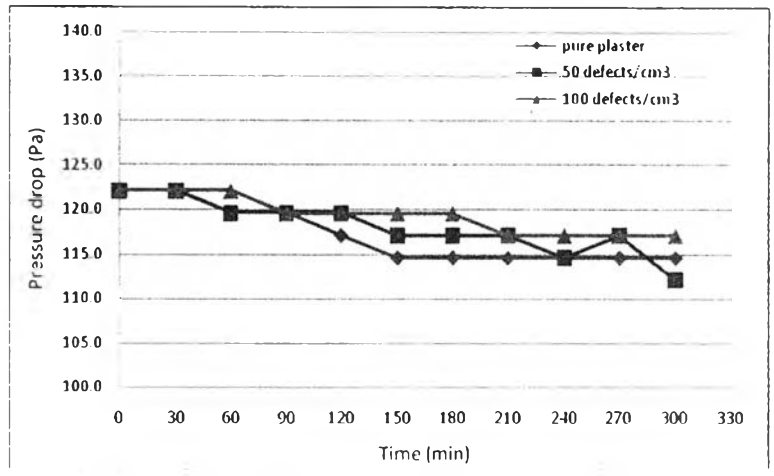

Figure 4.31 Pressure drop with time at different concentrations of particles, 0.42-0.50 mm, 25°C and 35 LPM.

4.3.5 The Effect of Temperature

Temperature has a significant effect on pressure drop at low flow rate. Higher temperature (25°C) of fluid shows a higher pressure drop than a lower temperature (10°C) as shown in Figures 4.32 and 4.33. At high flow rate (35LPM) as shown in Figure 4.33, temperature has no significant effect on pressure drop. Pressure drops also tend to decrease with time. Pressure drop at high flow rate was more stable than at low flow rate.

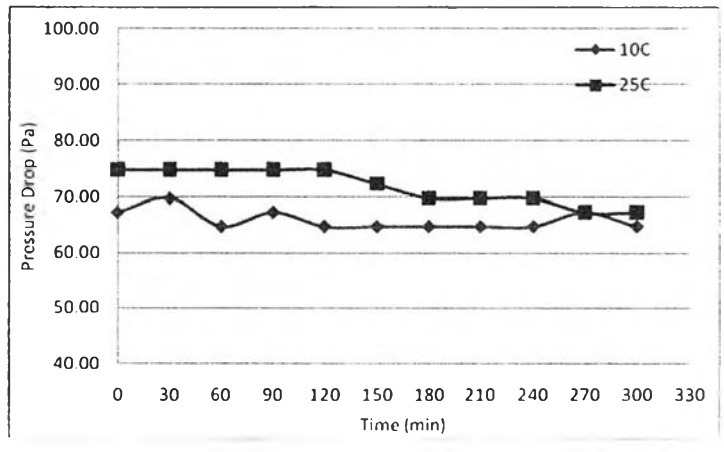

Figure 4.32 Pressure drop with time at different temperatures, 0.21-0.25 mm, 50 defects/cm^3 and 25 LPM.

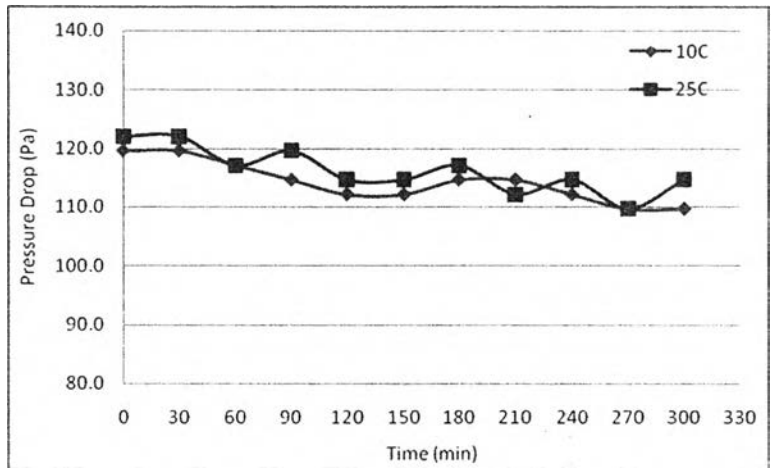

Figure 4.33 Pressure drop with time at different temperatures, 0.21-0.25 mm, 50 defects/cm^3 and 35 LPM.

4.4 The Mechanism of Gypsum Dissolution

The overall rate constant (K), mass transfer coefficient (k_m) and dissolution coefficient (k_d) were determined to understand the mechanism of gypsum dissolution. The overall rate constant is the proportionality constant between the reaction rate and the concentration of reactants. It was determined from the dissolution rates along the pipe measured at the end of the test. The mass transfer coefficient was determined in the plaster pipe by the correlations between the Stanton number, Reynolds number and Schmidt number over the range of $8 \times 10^3 < Re < 2 \times 10^5$ and Schmidt number between 1000 – 6000. The dissolution coefficient was determined from the relationships between the overall rate constant and the mass transfer coefficient. The entrance section and the fully-develop region were considered to understand the different mechanisms at different regions of flow. Different temperatures and different flows show the different fully develop length.

4.4.1 The Effect of pH

Figure 4.34 to Figure 4.36 show the results of the overall rate constant (K) and the dissolution coefficient (k_d) compared with the mass transfer coefficient (k_m) at different pHs.

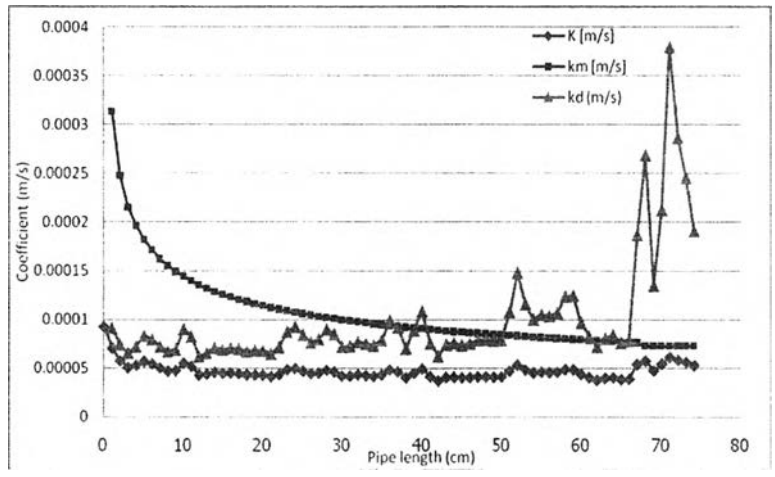

Figure 4.34 The overall rate constant (K) and the dissolution coefficient (k_d) compared with the mass transfer coefficient (k_m) along the pipe under condition pH3, 30°C and 25 LPM

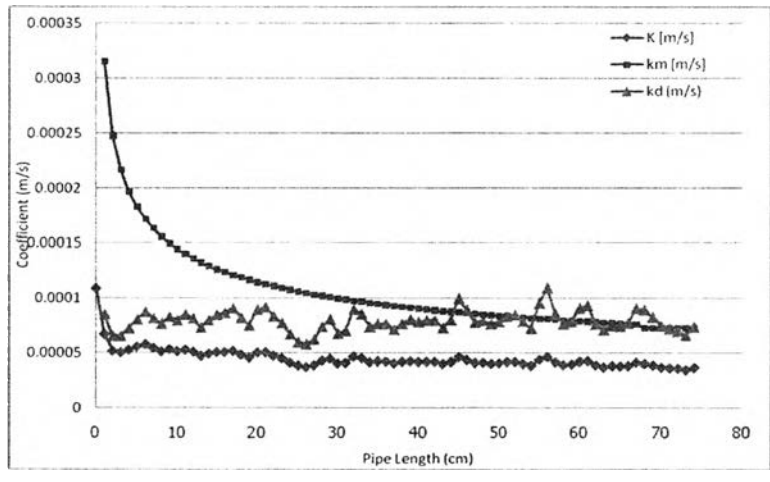

Figure 4.35 The overall rate constant (K) and the dissolution coefficient (k_d) compared with the mass transfer coefficient (k_m) along the pipe under condition pH7, 30°C and 25 LPM

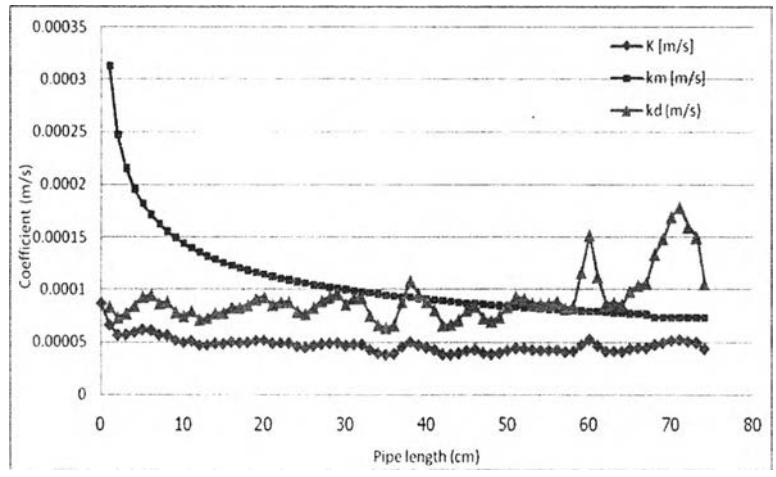

Figure 4.36 The overall rate constant (K) and the dissolution coefficient (k_d) compared with the mass transfer coefficient (k_m) along the pipe under condition pH10, 30°C and 25 LPM

4.4.2 The Effect of Flow Rate

Figure 4.37 and Figure 4.38 show the results of the overall rate constant (K) and the dissolution coefficient (k_d) compared with the mass transfer coefficient (k_m) at different flow rates.

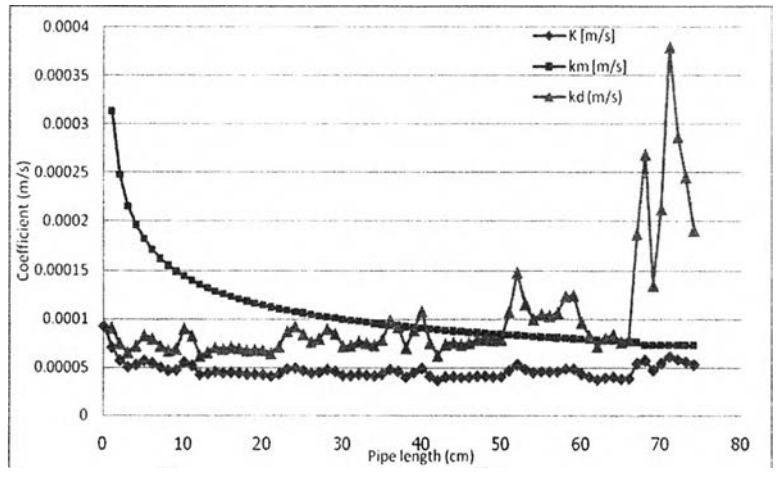

Figure 4.37 The overall rate constant (K) and the dissolution coefficient (k_d) compared with the mass transfer coefficient (k_m) along the pipe under condition pH3, 30°C and 25 LPM

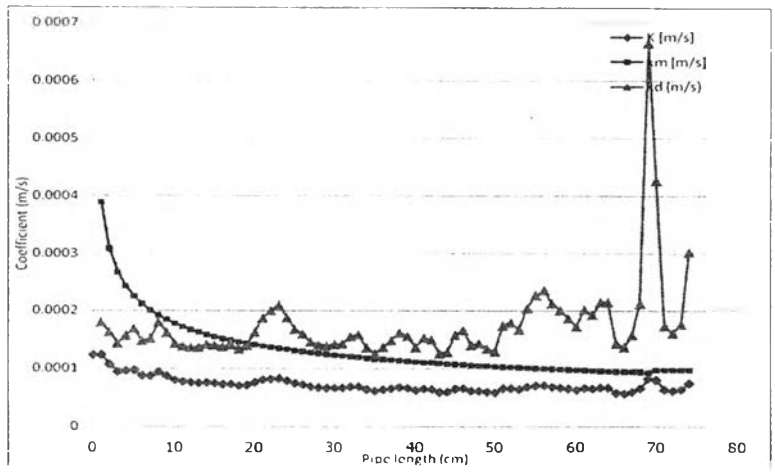

Figure 4.38 The overall rate constant (K) and the dissolution coefficient (k_d) compared with the mass transfer coefficient (k_m) along the pipe under condition pH3, 30°C and 35 LPM

Table 4.10 shows the values of the overall rate constant, the mass transfer coefficient and the dissolution coefficient at different pHs and different flow rates.

Table 4.10 Values of the overall rate constant, mass transfer coefficient and dissolution coefficient at different pHs.

pH	Flow rate (LPM)	K (m/s)	k_m (m/s)	k_d (m/s)	Flow rate (LPM)	K (m/s)	k_m (m/s)	k_d (m/s)
3	25	4.65E-05	1.07E-04	9.96E-05	35	7.11E-05	1.33E-04	1.75E-04
7	25	4.68E-05	1.08E-04	9.37E-05	35	7.10E-05	1.33E-04	1.92E-04
10	25	4.67E-05	1.07E-04	9.16E-05	35	7.16E-05	1.32E-04	1.84E-04

4.4.3 The Effect of Particle Size

Figures 4.39 to 4.41 show the results of the overall rate constant (K) and the dissolution coefficient (k_d) compared with the mass transfer coefficient (k_m) at different sizes of particle.

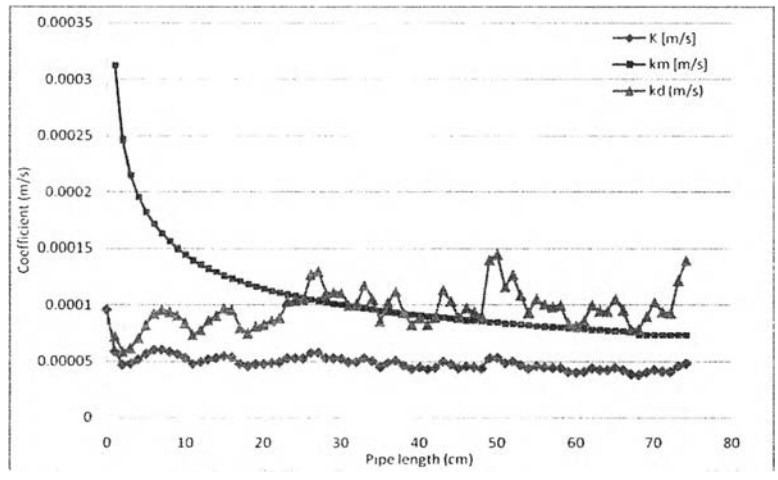

Figure 4.39 The overall rate constant (K) and the dissolution coefficient (k_d) compared with the mass transfer coefficient (k_m) along the pipe under condition 0.21-0.25mm, 50 defects/cm^3, 25°C and 25 LPM.

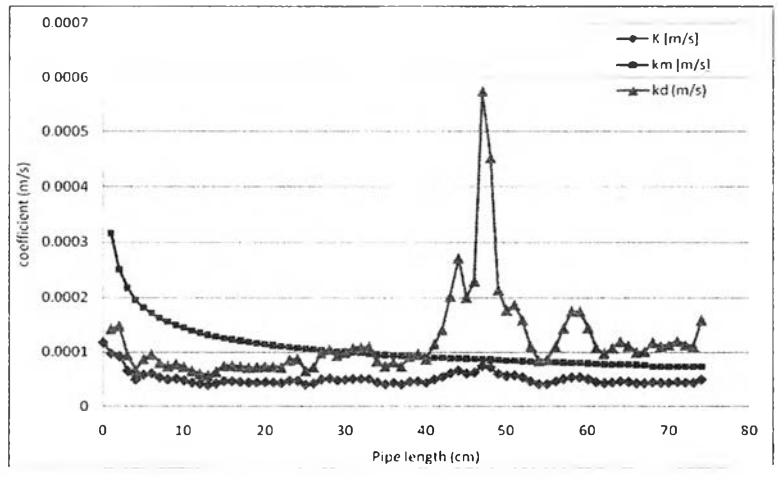

Figure 4.40 The overall rate constant (K) and the dissolution coefficient (k_d) compared with the mass transfer coefficient (k_m) along the pipe under condition 0.42-0.50mm, 50 defects/cm^3, 25°C and 25 LPM.

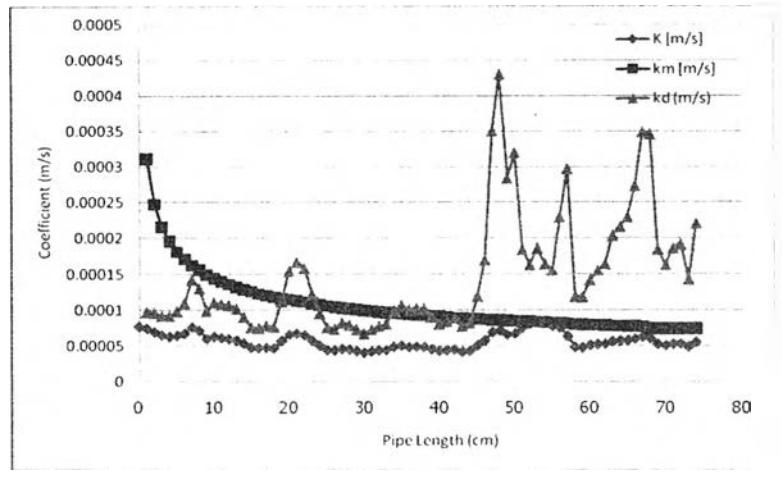

Figure 4.41 The overall rate constant (K) and the dissolution coefficient (k_d) compared with the mass transfer coefficient (k_m) along the pipe under condition 0.500-0.707 mm, 50 defects/cm^3, 25°C and 25 LPM.

4.4.4 The Effect of Particle Concentration

Figures 4.42 to 4.43 show the results of the overall rate constant (K) and the dissolution coefficient (k_d) compared with the mass transfer coefficient (k_m) at different concentrations of particles.

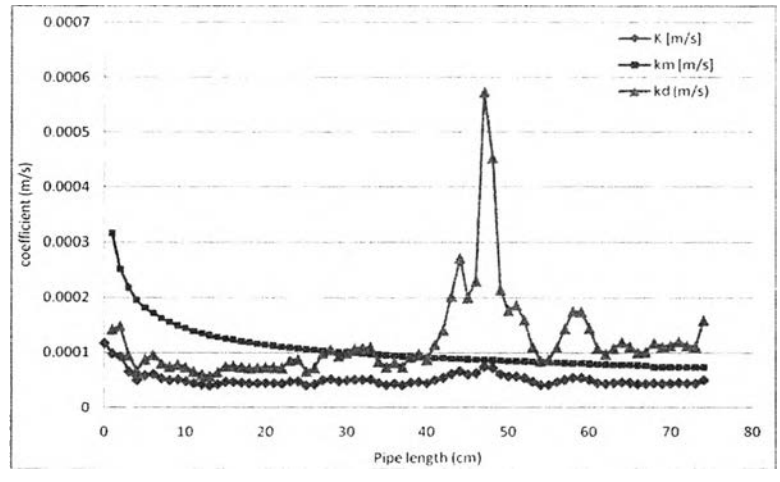

Figure 4.42 The overall rate constant (K) and the dissolution coefficient (k_d) compared with the mass transfer coefficient (k_m) along the pipe under condition 0.42-0.50mm, 50 defects/cm^3, 25°C and 25 LPM.

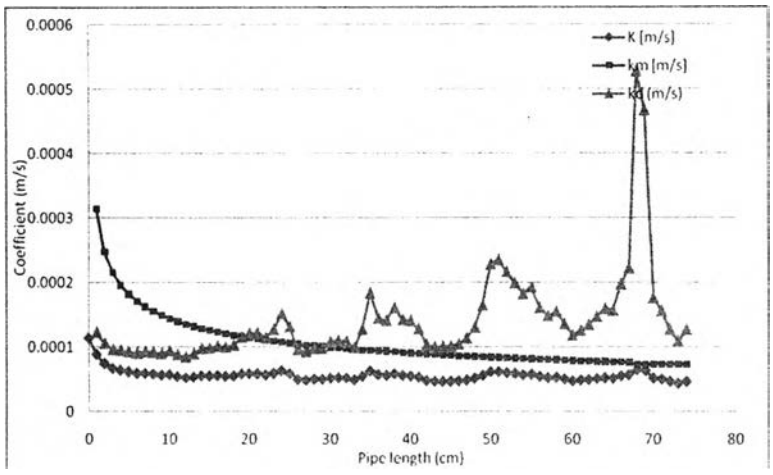

Figure 4.43 The overall rate constant (K) and the dissolution coefficient (k_d) compared with the mass transfer coefficient (k_m) along the pipe under condition 0.42-0.50mm, 100 defects/cm^3, 25°C and 25 LPM.

Table 4.11 shows the average values of the mass transfer coefficient and the dissolution coefficient at different surface roughness.

Table 4.11 Average values of mass transfer coefficient and dissolution coefficient at different surface roughness.

Defect Size (mm)	Defect Conc. (defects/cm^3)	Flow rate (LPM)	K (m/s)	k_m (m/s)	k_d (m/s)	Flow rate (LPM)	K (m/s)	k_m (m/s)	k_d (m/s)
Pure Plaster	0	25	4.43E-05	1.07E-04	8.68E-05	35	6.97E-05	1.32E-04	1.91E-04
0.21-0.25	50	25	4.83E-05	1.07E-04	9.63E-05	35	7.73E-05	1.32E-04	2.26E-04
	100	25	5.07E-05	1.07E-04	1.08E-04	35	7.92E-05	1.32E-04	2.66E-04
0.42-0.50	50	25	5.09E-05	1.07E-04	1.21E-04	35	8.39E-05	1.32E-04	3.12E-04
	100	25	5.52E-05	1.07E-04	1.40E-04	35	8.63E-05	1.32E-04	3.83E-04
0.500-0.707	50	25	5.66E-05	1.07E-04	2.12E-04	35	8.90E-05	1.33E-04	4.14E-04
	100	25	6.28E-05	1.07E-04	2.50E-04	35	9.28E-05	1.32E-04	5.34E-04

4.4.5 The Effect of Temperature

Figures 4.44 and 4.45 show the overall rate constant (K) compared with mass transfer coefficient (k_m) along the pipe.

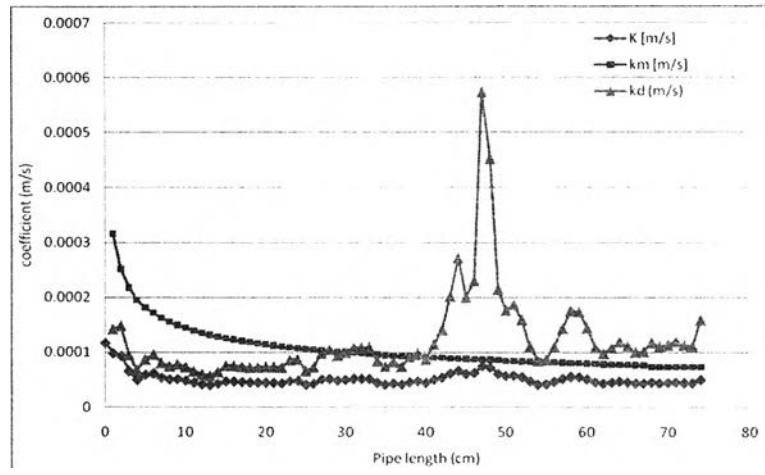

Figure 4.44 The overall rate constant (K) and the dissolution coefficient (k_d) compared with the mass transfer coefficient (k_m) along the pipe under condition 0.42-0.50mm, 50 defects/cm^3, 10°C and 25 LPM.

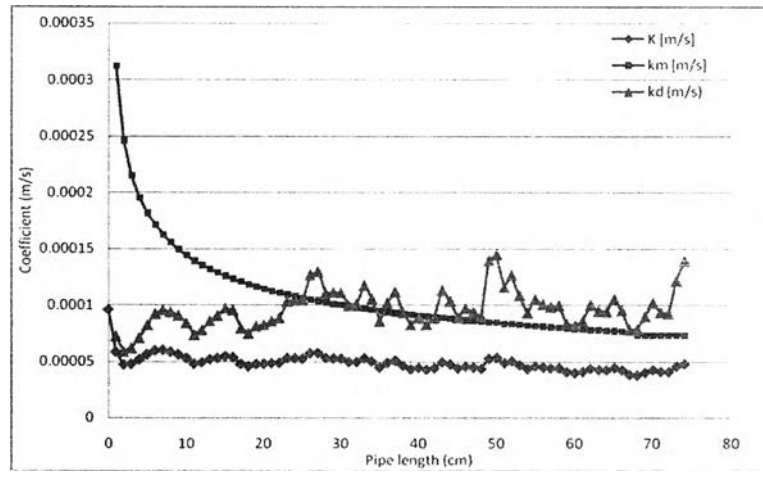

Figure 4.45 The overall rate constant (K) and the dissolution coefficient (k_d) compared with the mass transfer coefficient (k_m) along the pipe under condition 0.42-0.50mm, 50 defects/cm^3, 25°C and 25 LPM.

Tables 4.12 and 4.13 show the average values of the mass transfer coefficient and the dissolution coefficient at different temperature of the bulk fluid.

Table 4.12 Average values of mass transfer coefficient and dissolution coefficient at different temperatures.

Defect Size (mm)	Defect Conc. (defects/cm^3)	Flow rate (LPM)	10°C			25°C		
			K (m/s)	k_m (m/s)	k_d (m/s)	K (m/s)	k_m (m/s)	k_d (m/s)
Pure Plaster	0	25	2.76E-05	6.55E-05	5.17E-05	4.43E-05	1.07E-04	8.68E-05
0.21-0.25	50	25	2.95E-05	6.51E-05	5.90E-05	4.83E-05	1.07E-04	9.63E-05
	100	25	3.08E-05	6.50E-05	6.66E-05	5.07E-05	1.07E-04	1.08E-04
0.42-0.50	50	25	3.37E-05	6.51E-05	9.74E-05	5.09E-05	1.07E-04	1.21E-04
	100	25	3.82E-05	6.51E-05	1.19E-04	5.52E-05	1.07E-04	1.40E-04
0.500-0.707	50	25	3.55E-05	6.52E-05	1.00E-04	5.66E-05	1.07E-04	2.12E-04
	100	25	4.65E-05	6.51E-05	1.46E-04	6.28E-05	1.07E-04	2.50E-04

Table 4.13 Average values of mass transfer coefficient and dissolution coefficient at different temperatures.

Defect Size (mm)	Defect Conc. (defects/cm^3)	Flow rate (LPM)	10°C			25°C		
			K (m/s)	k_m (m/s)	k_d (m/s)	K (m/s)	k_m (m/s)	k_d (m/s)
Pure Plaster	0	35	4.20E-05	8.03E-05	1.01E-04	6.97E-05	1.32E-04	1.91E-04
0.21-0.25	50	35	4.66E-05	8.03E-05	1.40E-04	7.73E-05	1.32E-04	2.26E-04
	100	35	4.93E-05	8.01E-05	1.94E-04	7.92E-05	1.32E-04	2.66E-04
0.42-0.50	50	35	5.23E-05	8.03E-05	2.03E-04	8.39E-05	1.32E-04	3.12E-04
	100	35	5.94E-05	6.07E-05	2.52E-04	8.63E-05	1.32E-04	3.83E-04
0.500-0.707	50	35	6.05E-05	6.07E-05	2.34E-04	8.90E-05	1.33E-04	4.14E-04
	100	35	6.33E-05	6.07E-05	2.92E-04	9.28E-05	1.32E-04	5.34E-04

4.5 Effects of Various Parameters on Dissolution

The results of the gypsum dissolution mechanism indicates that the entrance effect impinged the mechanism of gypsum dissolution. The dissolution coefficient is lower than the mass transfer coefficient at this region. This means surface reaction is a rate-limiting step because the boundary layer has not developed or is being developed. Hence, the surface reaction is the main mechanism of dissolution in this section. The diffusion of the dissolved species through the boundary layer is very effective so that the concentration at the surface will approach the one in the bulk. During developing of the boundary layer, the dissolution coefficient gradually increases while the mass transfer coefficient decreases. The transport of the reactants or products through the boundary layer is less effective and becomes the slowest step. The mechanism becomes under transport control. A change in thickness of the boundary layer affects the diving force (concentration gradients) for the dissolution of soluble surface through the layer. The dissolution coefficient shows some apparent peaks at some points along the pipe length. This is due to the values of the overall rate constant are close to the mass transfer coefficient ($K=k_m$). Hence, the dissolution coefficient must show much higher value than the mass transfer coefficient to neglect $1/k_d$ term to give the equation (5.3d) to be corrected. However, the dissolution of gypsum is controlled by both surface reaction and diffusion transport through the boundary layer. Therefore, dissolution rate of gypsum is then controlled by mixed-kinetics.

Both the overall rate constant and the dissolution coefficient show the similar results at different pH. This indicates that pH has no effect on the dissolution mechanism of gypsum. The overall rate constant and the dissolution coefficient correlate with flow rate. Both increase with flow rate. Moreover, the results show a significant effect of surface roughness on the coefficients. The overall rate constant and the dissolution coefficient increase with increasing surface roughness and temperature. This is due to the higher rate of dissolution. This indicates that at greater surface roughness, a higher dissolution rate was obtained.

Dissolution rates were compared under different conditions to observe the effects of parameters on the dissolution rate and mechanism of dissolution. Table

4.14 shows the dissolution rate for different flow rates and different temperatures. It was found that the dissolution rate could be changed more than 50% by increasing the temperature, whereas the dissolution rate could be changed more than 40% by increasing flow rate. This results from the solubility of plaster at different temperatures, which decreases 7.19% between 25°C to 10°C (Azimi *et al*, 2007). This indicates that temperature has more effect on the dissolution rate than the effect of flow rate.

Table 4.14 Dissolution rate comparison between the effect of flow rate and effect of temperature.

Conditions	Pure Plaster	0.21-0.25 mm 50 defects/cm^3	0.21-0.25 mm 100 defects/cm^3	0.42-0.50 mm 50 defects/cm^3	0.42-0.50 mm 100 defects/cm^3	0.500-0.707 mm 50 defects/cm^3	0.500-0.707 mm 100 defects/cm^3
25LPM_25C	1.867	1.974	2.048	2.076	2.133	2.246	2.466
25LPM_10C	1.052	1.109	1.103	1.222	1.250	1.295	1.386
% Difference	55.83	56.15	59.96	51.80	52.17	53.67	56.09
35LPM_25C	2.883	3.136	3.136	3.484	3.579	3.770	3.920
35LPM_10C	1.576	1.734	1.806	1.996	2.027	2.194	2.407
% Difference	58.62	57.56	53.85	54.34	55.37	52.86	47.81
25LPM_25C	1.867	1.974	2.048	2.076	2.133	2.246	2.466
35LPM_25C	2.883	3.136	3.136	3.484	3.579	3.770	3.920
% Difference	42.77	45.47	41.99	50.66	50.66	50.67	45.53
25LPM_10C	1.052	1.109	1.103	1.222	1.250	1.295	1.386
35LPM_10C	1.576	1.734	1.806	1.996	2.027	2.194	2.407
% Difference	39.86	44.01	48.31	48.10	47.43	51.50	53.86

Table 4.15 shows the rates of dissolution compared between the initial defect sizes and the initial defect concentrations, based on the dissolution rate of pure plaster. It was found that the dissolution rate is higher when initial defects are added. Defect concentration has a greater effect on dissolution rate than defect size. This means more scallops can be initiated by increasing the defect concentration than increasing the size of the defects. Consequently, the surface area of the plaster increases and the dissolution rate increases. This supports the Defect theory.

Table 4.15 Dissolution rate comparison between the effect of initial defect size and effect of initial defect concentration.

Conditions	Pure Plaster	0.21-0.25 mm 50 defects/cm^3	0.21-0.25 mm 100 defects/cm^3	0.42-0.50 mm 50 defects/cm^3	0.42-0.50 mm 100 defects/cm^3	0.500-0.707 mm 50 defects/cm^3	0.500-0.707 mm 100 defects/cm^3
25LPM_25C	0	1.974	2.048	1.076	2.133	2.246	2.466
% Difference	-	5.76	9.70	11.21	14.24	20.30	32.12
25LPM_10C	0	0.680	1.113	1.222	1.250	1.295	1.386
% Difference	-	5.38	5.79	16.13	18.82	23.12	31.72
35LPM_25C	0	3.073	3.136	3.384	3.579	3.770	3.920
% Difference	-	10.18	8.79	20.88	24.18	30.77	35.99
35LPM_10C	0	1.734	1.806	1.996	2.027	2.194	2.407
% Difference	-	10.05	14.57	26.63	28.64	39.20	52.76